Journal of Power Sources 196 (2011) 741–746

Contents lists available at ScienceDirect

Journal of Power Sources

journal homepage: www.elsevier.com/locate/jpowsour

Superefficient thin film multilayer catalyst for generating hydrogen from sodium borohydride

Lunghao Hu [a,b,*], R. Ceccato [a], R. Raj [b,1]

[a] Department of Materials Engineering and Industrial Technologies, University of Trento, Via Mesiano 77, 38123 Trento, Italy
[b] Department of Mechanical Engineering, University of Colorado, Boulder, CO 80309-0427, USA

ARTICLE INFO

Article history:
Received 10 June 2010
Received in revised form 22 July 2010
Accepted 24 July 2010
Available online 1 August 2010

Keywords:
Sodium borohydride
Functionalized carbon nanotube
Ternary catalyst
Electrophoretic deposition
Hydrogen generation
Silicon carbonitride

ABSTRACT

A multilayer catalyst consisting of a electrophoretically deposited thin film of carbon nanotubes (CNTs) on a substrate of carbon fibers, followed by a coating of polymer-derived silicon carbonitride (SiCN), which is then decorated with a monolayer of transition metals is shown to perform at the upperbound of the phenomemological prediction from an earlier work [1]. A figure-of-merit for first order kinetics is equal to 4600 L min^{-1} $[NaBH_4]^{-1}$ $g_{met}{}^{-1}$, which is nearly 30 times the value reported in literature, is achieved. This high FOM is attributed to the CNT-thin film, as opposed to the thick CNT-paper used in previous work, thus needing merely 0.15 wt% quantities of precious metals for effective catalysis. This new architecture corroborates the concepts that: (i) the catalytic activity derives mainly from the surface of the CNT substrate, and (ii) the silicon carbonitride interlayer is instrumental in dispersing the transition metals into a monolayer. The hydrogen generation rate (HGR) for zero order kinetics, which is obtained when $[NaBH_4] > 0.03$ M, is measured to be 75 L min^{-1} $g_{met}{}^{-1}$, which is among the higher values reported in the literature. The present multilayer catalysts are able to perform without fading for many cycles, presumably because the bondings in the substrate are predominantly covalent. This feature adds further uniqueness to this multilayer catalyst.

1. Introduction

This work belongs to a series of papers that demonstrate the viability of a novel architecture of a catalyst for generating hydrogen from an alkaline aqueous solution of sodium borohydride. The basic premise of this design, described in Ref. [1,2], is that a thin coating of polymer-derived silicon carbonitride applied to carbon nanotubes permits the dispersion of transition metals as a monolayer on the surface of the catalyst, the argument being that the strong bonding between these metals and silicon, as known from the high energy of formation of silicides, would enhance wetting and greatly retard surface diffusion, thereby preventing the growth of nanoclusters of the metals. In the limit the metals can be expected to form a monolayer, or a picoscale catalyst, as illustrated in Fig. 1, so that all metal atoms may participate in the catalytic process. Two additional criteria for high catalytic activity were proposed. First, that the substrate should have a high surface area, and second, that it should be electronically conductive [1]. In the first instance a CNT-paper, several tens of micrometers thick, appeared not only to fulfill these requirements but it also provided physical strength to the catalyst for handling and working.

A parametric description of the performance of a catalyst is related to the order of the reaction kinetics. In first order kinetics, the hydrogen generation rate is proportional to the molar concentration of $NaBH_4$ in the solution, which when normalized with respect to the weight of the precious metal, leads to the following measure of performance, which we have called the figure-of-merit, or FOM, having the units: L min^{-1} $[NaBH_4]^{-1}$ $g_{met}{}^{-1}$, where g_{met} is the weight of the precious metal in g.

At high concentrations of $NaBH_4$, the kinetics usually transitions from first order to zero order. In this case the hydrogen generation rate is independent of $[NaBH_4]$. The hydrogen generation rate, or HGR, now has units of L min^{-1} $g_{met}{}^{-1}$. While HGR is usually more important in applications, the first order rate constant, and especially the transition from first order to zero order with the change in concentration is important for a scientific understanding of the catalytic mechanism, and for reliable and predictable operation of the catalyst.

The HGR can be converted into power generation in fuel cells by assuming a value of the cell voltage. If the cell voltage is 0.7 V then hydrogen generation rate of 1 L min^{-1} is equivalent to the production of 100 W of energy. Therefore, if the HGR is 100 L min^{-1} $g_{met}{}^{-1}$ it would mean that 10 kW of energy would require 1 g of precious metal.

* Corresponding author at: Department of Mechanical Engineering, University of Colorado, Boulder, CO 80309-0427, USA. Tel.: +1 303 735 2651; fax: +1 303 492 3498.
E-mail addresses: lung.hu@colorado.edu, lunghao.hu@gmail.com (L. Hu).
[1] RR is affiliated with PDC-Energy, LLC, Louisville, CO, USA.

0378-7753/$ – see front matter © 2010 Elsevier B.V. All rights reserved.
doi:10.1016/j.jpowsour.2010.07.070

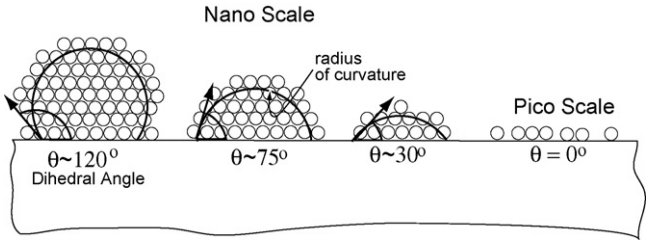

Fig. 1. The influence of contact angle on the surface to volume ratio of the cluster. Elemental or picoscale dispersion of the metal atoms can be obtained if the contact angle approaches zero; from Ref. [1].

In Ref. [1], where CNT-paper was used as the substrate, an FOM of 150–300 L min^{-1} $[NaBH_4]^{-1}$ $g_{met}{}^{-1}$, and HGR of 15 L min^{-1} $g_{met}{}^{-1}$ was obtained. By employing a thin film of CNTs, deposited on a carbon-fiber substrate we show that values of 4600 L min^{-1} $[NaBH_4]^{-1}$ $g_{met}{}^{-1}$, and 75 L min^{-1} $g_{met}{}^{-1}$, for FOM and HGR have been obtained. The transition from first order to zero order occurred at approximately $[NaBH_4] > 0.03$ M.

The measurement of the FOM from Ref. [1] is compared with the data from literature in Fig. 2. In this log–log plot the FOM is plotted against the size of the metal cluster, ranging from atom size, or 100 pm up to 100,000 pm, that is from 0.1 nm to 100 nm, so that the lower limit corresponds to a monolayer. Since the surface of volume of clusters is inversely proportional to their size, a trend line with a slope of unity was drawn through the data available in the literature. It is not surprising that the data do not fall directly on this trend line since the surface to volume ratio would depend not only on the cluster size but also on the contact angle made by the cluster with the substrate (Fig. 1). Additionally the metal chemistry would also affect the catalytic efficiency. Nevertheless the line shown in Fig. 2 does give a phenomenological trend to the data. The result obtained in Ref. [1] is shown in this figure by assuming that the metals formed a monolayer, that is for a size of 100 pm. The FOM obtained in [1], using a ~150 μm thick CNT-paper as the substrate was 175–300 L min^{-1} $g_{met}{}^{-1}$ $[NaBH_4]^{-1}$, as marked in Fig. 2. This value fell one to two orders of magnitude below the value expected from the trend line for a monolayer catalyst. In this first paper a binary catalyst made from Pd/Pt was employed. The

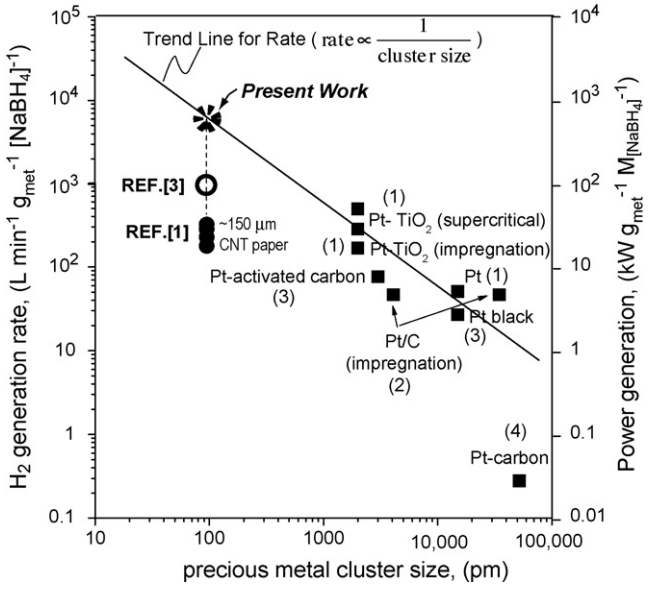

Fig. 2. A plot of the figure-of-merit for the catalyst as a function of the cluster size of the metal atoms showing the evolution of the CNT/SiCN/Metal based catalyst from Ref. [1], to [3], to the present work.

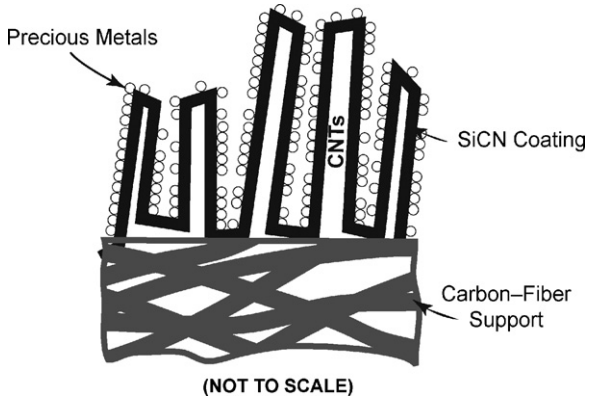

Fig. 3. The four-layer catalyst architecture.

unique result of the present work is that the phenomenologically predicted upperbound in Ref. [1] is indeed achieved as marked in Fig. 2.

We hypothesized that the shortfall relative to the predicted performance in the 150 μm CNT-paper catalyst arose from the trapping of hydrogen bubbles generated within the paper by the mesh-like network of the carbon nanotubes. Thus all the metal atoms were not being effectively used for catalysis, thereby lowering the overall figure-of-merit. The next phase of this work focused on working with thinner CNT-paper. Results obtained with 25 μm thick paper [3], with a ternary Pt/Pd/Ru catalyst gave a figure-of-merit value of 900 L min^{-1} $g_{met}{}^{-1}$ $[NaBH_4]^{-1}$, six times the value from [1] but still short of the phenomenologically predicted upper bound. The 25 μm paper was the thinnest possible, free-standing catalyst that could be physically made and handled.

Further evolution of this architecture is presented in this article. Here the CNT was deposited as a thin film on a carbon-fiber substrate (CF) by electrophoresis. The carbon nanotubes were dispersed in a strongly oxidizing solution which is known to grow oxygen bonds on the edges of the nanotubes [4–8], making them polar, and therefore amenable to electrophoretic deposition (after electrophoretic deposition the sample is heated to 1100 °C which decomposes the –C=O bonds back into sp^2 carbon). The remaining procedure for preparing the catalyst was similar to that reported in Ref. [3], which includes coating of a polymer-derived silicon carbonitride (SiCN) followed by deposition of atoms of precious metals. In this way, the catalyst is designed to have a four-layer architecture as illustrated in Fig. 3: it consists of a carbon-fiber substrate, coated with a thin films of CNTs, which are coated with (a monolayer) of SiCN, followed by a submonolayer of metal atoms. This new catalyst gave a FOM equal to 4600 L min^{-1} $g_{met}{}^{-1}$ $[NaBH_4]^{-1}$, lying close to the upperbound value predicted by the trend line in Fig. 2.

The following sections describe the experimental procedure for preparing this multilayer architecture [1,3]. We ascribe the high value of FOM simply to the thin film nature of the CNT, which permits free evolution of hydrogen (as opposed to trapping of bubbles within the CNT-paper), rather than to a fundamentally different mechanism than described in [1,3]. The reader is referred to these papers for a discussion of the proposed catalytic mechanism.

2. Preparation of catalysts

2.1. Electrophoretic deposition of carbon nanotubes on carbon-fiber substrate

Single-walled CNT were acquired as "Purified HIPCO® Single-Wall Carbon NanoTubes", from Unidym CA, USA. The procedure

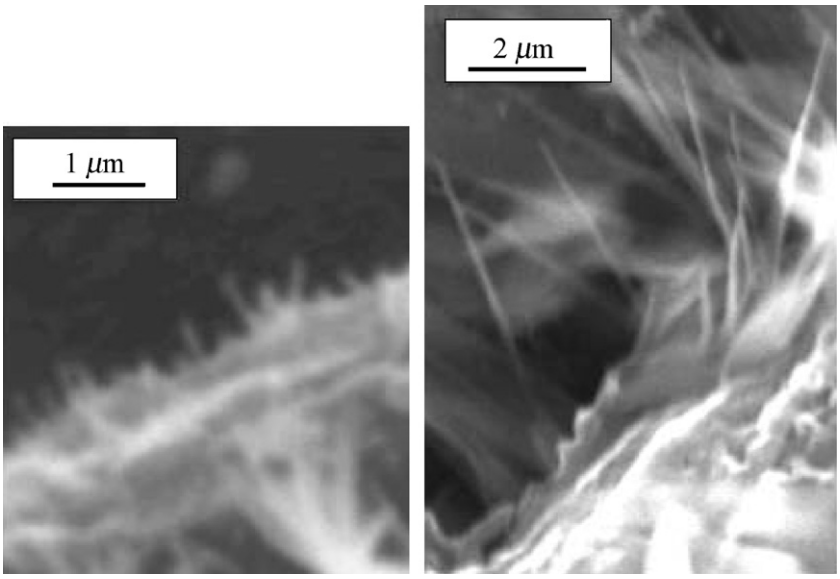

Fig. 4. SEM micrographs of CNT-thin film deposited on carbon-fiber substrate. On the left the CNTs appear to be deposited as single tubes, while on the right they are in the form of bundles. Note that the CNTs project outwards from the surface of the carbon fibers, as shown schematically in Fig. 3.

described in [9–15] was used for dispersing and electrophoretic deposition of the tubes. The as-received tubes were dispersed in a mixture of concentrated nitric and sulphuric acids in a ratio of 1:3. Thirty milligrams of the single-wall CNTs were added to 4 mL acid mixture. The mixture was refluxed for 1 h at 130 °C. One mL of this solution was extracted, to which 1 M solution of NaOH was added until the pH reached a slightly basic value. At this point the solution the solution became clear, with a yellowish tinge. The adjustment of the pH towards basic causes the migration of the CNTs towards the positive electrode upon application of a DC field (it has been shown that replacing NaOH with by salts causes deposition towards the negative electrode [15]). Electrodeposition was carried out with two, 4 cm^2 carbon-fiber electrodes (Toray carbon-fiber paper), immersed into the nanotube solution, held 5 mm apart. A DC voltage (10 V) was applied for 5 min to achieve deposition of the CNTs. Scanning electron microscope micrographs of the CNT coating are shown in Fig. 4. They show (apparently) single carbon nanotubes as well as bundles of nanotubes growing approximately normal to the substrate. The thickness of the film lies in the 100 nm to 1 μm range.

2.2. Coating with silicon carbonitride

At this point the catalyst was ready for depositing a coating of silicon carbonitride, and then with Pt/Pd/Ru metal catalyst, a procedure similar to that described in [3]. Briefly, the carbon-fiber paper coated with CNT-thin film, CF/CNT was, at first, functionalized by dip-coating into a commercial polymer-derived ceramic solution, Ceraset from Kion, Germany, diluted with acetone to 10 wt% and then pyrolyzed at 1100 °C for 3 h under flowing Ar [16]. In the final step, the metals were deposited on the SiCN surface in the following way.

2.3. Metal elements

First, ionic solutions of the metals were prepared with 100 mL of 40 mM chloroplatinic acid hexahydrate solution ($H_2PtCl_6{\cdot}6H_2O$, ABCR), 100 mL of 40 mM acidic $PdCl_2$ solution (40 mL of 1 M HCl and 60 mL of deionized water), and 100 mL of 20 mM of $RuCl_3{\cdot}xH_2O$ solution. Pt metal ions were protected by poly (N-vinyl-2-pyrrolidone, PVP, Mw = 40,000) by refluxing 1 mL of Pt ionic solution in 60 mL of alcohol (methanol or 1-propanol mixed with water) at 110 °C for 3 h. During refluxing the color of the solution changed from pale yellow to dark brown [17]. Pd and Ru solutions were also prepared by first protecting with poly (N-vinyl-2-pyrrolidone, PVP, Mw = 40,000) and mixing with diluted alcohol, but the metal solution was made by reducing the metal salts with by sodium borohydride [18–21], since refluxing temperatures to create the metal solutions were much higher than for Pt. The metals were deposited from these three metal solutions by electrolytic transport. A pair of CF/SiCN/CNT substrates samples were immersed into each metal suspension and kept at a fixed gap distance, 5 mm. A 20 V DC voltage was applied between these two electrodes for 10 min for each metal suspension [17]. The resulting CF/CNT/SiCN/(Pt/Pd/Ru) catalyst was ready for hydrogen generation experiments. The same catalyst could be used several times for the experiments, with reproducible results, without any evidence of degradation in performance.

3. Measurements

3.1. Measurement of metal content

Elemental analysis of the metal content was carried out with Inductively Coupled Plasma ICP-OES Ciros Spectro instrument. Selected wavelengths for metals were set at 214.423 nm (Pt), 340.458 nm (Pd) and 240.272 nm (Ru). Fragments of the catalyst samples were weighed and the metals were extracted by dissolving in "aqua regia" (HCl/HNO_3, 3/1, v/v) solutions, which were analyzed by ICP. The % metal weight (as a fraction of the total weight of the catalyst, including the carbon-fiber support) was determined to be as follows: 0.055 wt% of Pt, 0.06 wt% of Pd and 0.03 wt% of Ru. It was not possible to measure the weight fraction of the CNT-thin film deposited on the carbon–fiber substrate since the before and after weight of the substrate upon electrophoretic deposition of the CNT-thin film was indistinguishable. It is estimated that the weight of the CNT film was less than 1 mg for a total weight of ~40 mg of the substrate.

3.2. Measurement of hydrogen generation

The volume of hydrogen generated was measured as a function of time, using a gas burette connected to the reaction flask. The

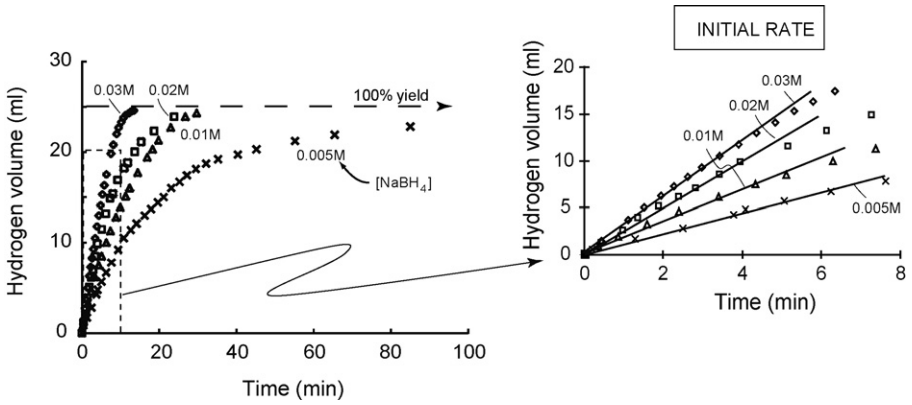

Fig. 5. The time dependent yield of hydrogen (left); the initial rates of hydrogen generation (right).

reaction was thermostated at fixed temperature 29–30 °C with a water bath. The sodium borohydride solution was stirred with a magnetic bar at 900 rpm to promote reaction between the solution and the catalyst. All experiments were carried out with an amount of sodium borohydride solution that would have a theoretical yield of 24 mL of hydrogen at NTP conditions. Four concentrations of sodium borohydride, 0.03 M, 0.02 M, 0.01 M and 0.005 M, respectively, were prepared. The solution was buffered with 1 M NaOH solution to pH 13. The total weight of catalyzed SiCN/CNT/CF sample was 40–42 mg.

4. Results and discussion

4.1. Kinetics

We follow here the procedure described in [1] for determining the zero order and the first order rate constants for hydrogen generation. The composite behavior is described by the following equation [1]:

$$\frac{1}{(dn_{H_2}/dt)} = \frac{1}{K_1}\frac{1}{[NaBH_4]g_{met}} + \frac{1}{K_2}\frac{1}{g_{met}} \quad (1)$$

Here dn_{H_2}/dt is the rate of production of moles of hydrogen, expressed here in units of mol min^{-1}, [$NaBH_4$] is the molar concentration of sodium borohydride at which the rate is measured, g_{met} is the weight of the metal elements present in the catalyst, K_1 is the first order rate constant, since it defines the proportionality between generation rate and molar concentration, and K_2 is the zero order rate since it gives the generation rate that remains independent of the molar concentration of sodium borohydride. Note that at high molar concentrations the first term on the right hand side becomes small compared to the second term, that is, the zero order rate constant dominates at high molar concentration.

The procedure for determining K_1 and K_2 is to plot the inverse of generation rate against the inverse of the molar concentration. Then, if Eq. (1) holds, the data would fit a straight line, the slope of which will yield K_1 and the intercept on y-axis will be equal to K_2. The rates are measured at the start of the experiment since these initial rates correspond to the initial molar concentrations that are known. Experiments were carried out at four different values of the initial concentration: from 0.03 M, 0.02 M, 0.01 M and 0.005 M sodium borohydride.

The plots in Fig. 5 give the time dependent yield of hydrogen. Note that in all cases the theoretically expected hydrogen is obtained, though the time constant, as expected from Eq. (1), depends on the molar concentration of $NaBH_4$. The inset in Fig. 5 shown in full scale on the right gives the initial rates of hydrogen generation. These initial rates are combined with the initial values

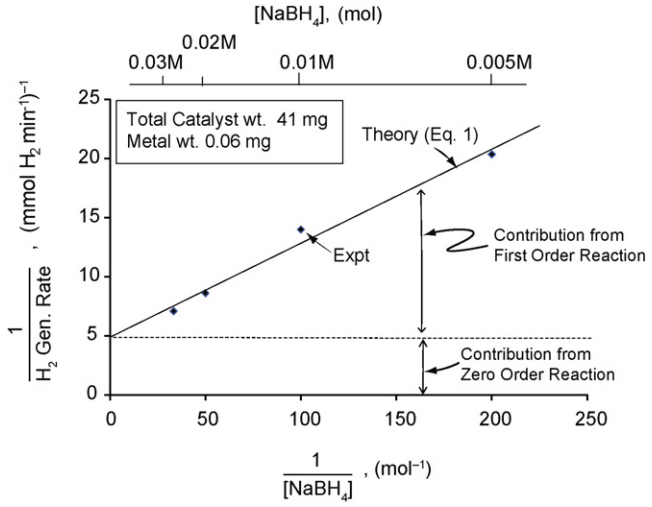

Fig. 6. A plot of initial values of the hydrogen generation rate (right hand plot in Fig. 5) according to Eq. (1). The slope of the fit to the data gives the first order rate constant, while the intercept on the y-axis provides the value for the zero order rate constant.

of [$NaBH_4$]; their inverse values are plotted against one another in Fig. 6, as guided by Eq. (1) (note that the slopes in Fig. 5 are in units of L min^{-1}: these have been converted to mol H_2 min^{-1} for Fig. 5 by dividing by 22.4 L mol^{-1}). The data in Fig. 6 give a reasonable linear fit. The intercept on the y-axis gives the zero order rate constant while the slope of the line gives the first order rate constant. These values are compared to the earlier data obtained with CNT-paper [1] in Table 1.

4.2. Figure-of-merit (FOM)

The graph in Fig. 6 suggests that at low molar concentration (e.g. 0.005 M [$NaBH_4$]) the hydrogen generation should follow first order kinetics. It is immediately shown that neglecting the zero order term in Eq. (1), integrating and recognizing that the rate of hydrogen generation is equal to the rate of consumption of [$NaBH_4$],

Table 1
A comparison of zero and first order rate constants from current experiments and Ref. [1].

	Ref. [1]	Present work
First order rate constant (mol H_2 min^{-1} g_{met}^{-1} [$NaBH_4$]$^{-1}$)	8–13	203
Zero order rate constant (mol H_2 min^{-1} g_{met}^{-1})	0.7	3.3

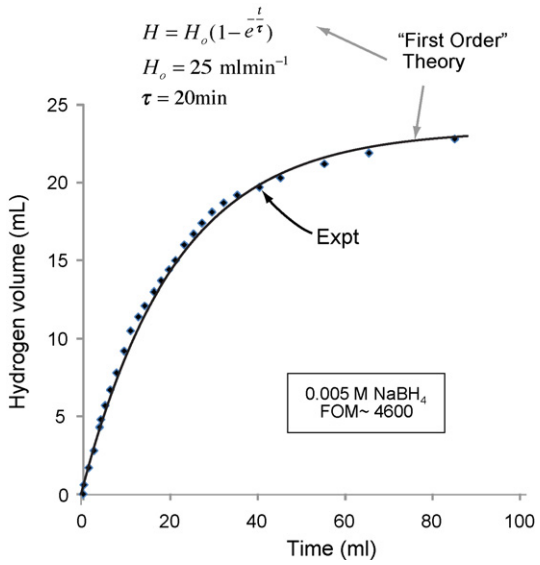

Fig. 7. The fit of the data for hydrogen evolution vs. time to (Eq. (2)), at the lowest concentration, where first order kinetics is expected to dominate. The fit confirms first order behavior.

gives an exponentially decreasing rate of hydrogen generation as given by the following result:

$$H = H_0(1 - e^{t/\tau}) \quad (2)$$

where H is the time dependent volume of hydrogen generated in the experiment, H_0 is the theoretical limit, and τ is the first order rate constant. The fit for Eq. (2) to the data for the 0.005 M [$NaBH_4$] experiment is shown in Fig. 7. This best fit of data and Eq. (2) is obtained for the time constant, $\tau = 20$ min.

Note that K_1 in Eq. (1) is also equal to the figure-of-merit in units of mol min^{-1} [$NaBH_4$]$^{-1}$ $g_{met}{}^{-1}$. Its value converted into L min^{-1} gives FOM = 4600 L min^{-1} [$NaBH_4$]$^{-1}$ $g_{met}{}^{-1}$.

4.3. Hydrogen generation rate (HGR)

The HGR is a critical engineering parameter to evaluate the catalytic efficiency. It is equal to the rate of hydrogen generation per unit weight of precious metals. It is self evident from Eq. (1) that with appropriate units it is the same as the zero order rate constant, K_2. Table 2 gives a comparison of HGR for the present work, and the data from literature. The order of catalytic reaction and the catalytic efficiency (FOM or HRG) are often complex, requiring a correlation to the concentration of $NaBH_4$, metal content, cluster size of the metal [31,32], the composition of the metal alloys [32–41], and the interaction between the metals, ligands and substrates [35,41]. In general the first or zero order is dominated by the concentration of the reactant and the catalyst content. The data from literature given in Table 2, therefore gives a general idea for the HGR, rather than measurements of the precise values for the zero order rate constant; generally speaking high loadings of the precious metals and high concentrations of $NaBH_4$ favor the zero order reaction.

The listings in Table 2 show that the present work lies among the top five measurements of HGR. However, certain aspects of the present work are unique. For example, the loading of the catalyst with precious metals is merely 0.15 wt%, far less than in the other high performance catalysts.

The present catalyst is highly stable and durable, performing without fading after several cycles and testing. This durability is ascribed to the highly covalent nature of the bonding in the present catalyst. Non-stoichiometry often leads to chemical changes: e.g. lithium cobalt oxide-based catalysts are likely to be vulnerable to changes in stoichiometry with use, since lithium is mobile at ambient temperature; non-s.

It is also noteworthy that a transition from first order to zero order behavior has been obtained at relatively low molar concentrations, [$NaBH_4$] > 0.03 M. At higher concentrations the generation rate is expected to be independent of concentration. Low concentrations can side step issues related to precipitation of salts at high concentrations, and corrosion, thereby offering the possibility of simpler and reliable designs of systems to deliver hydrogen to fuel cells.

4.4. Multilayer architecture of the catalyst and mechanism

The most important design features of this catalyst are:

(i) Using a thin film of CNTs, deposited on a carbon-fiber substrate: in the case of CNT-paper employed in [1,3] the interior of the paper may have trapped hydrogen bubbles thereby lowering the overall catalytic efficiency.
(ii) The SiCN interlayer between the CNTs and the metal atoms on the surface is needed to disperse the metal atoms into a monolayer thereby increasing the catalytic activity of the metal content to its highest possible level. In earlier work polymer-derived SiCN was shown to form a continuous layer on CNTs [16]. This layer is expected to form strong bonds with the precious metals, as in silicides, which retards surface diffusion, and improves wetting by lowering the contact angle. This mechanism is deemed to be essential to creating a monolayer of the metal atoms on the surface of the catalyst.
(iii) The CNT/SiCN layer is electronically conducting [16]. The electronic conductivity provides a pathway for electron transfer from $BH_4{}^-$ ion: the negative charge on $BH_4{}^-$ ion is transferred to one hydrogen atom, which is reduced by water molecules

Table 2
The comparison of HGR with different catalysts. Some data from this table are cited from [29].

Catalyst chemistry	Ref.	Temperature (°C)	HGR (L(H_2) min^{-1} $g_{met}{}^{-1}$)	Power generation (kW $g_{met}{}^{-1}$ (at 0.7 V))
0.15 wt% Pt/Pd/Ru/thin SiCN-CNT film	Present work	29	75	7.5
1.13 wt% Pt/Pd/Ru/25 μm SiCN/CNT/CF	[3]	29	21	2.1
1.07 wt% Pt/Pd/Ru 75 μm SiCN/CNT/CF	[3]	29	15	1.5
1.4 wt% PtPd/CNT	[1]	29	15	1.5
16.6 wt% $Ru_{60}Co_{20}Fe_{20}$/carbon fiber	[22]	20	42	4.2
13.3 wt% $Ru_{75}Co_{25}$/CF	[22]	20	37	3.7
1 wt% RuPt/TiO_2	[23]	20	10	1
10 wt% PtRu/Co_3O_4	[24]	25	85	8.5
2 wt% Ru/C	[25]	20	35	3.5
20 wt% Pt/C	[26]	20	115	11.5
10 wt% Ru/$LiCoO_2$	[27]	25	428	42.8
15 wt% Pt/$LiCoO_2$	[28]	20	367	36.7
10 wt% Pt/Ru/$LiCoO_2$	[24]	25	53	5.3
3 wt% Ru/graphite	[30]	30	32	3.2

in $NaBH_4$ hydrolysis. A detailed model for this mechanism is presented in Ref. [1].

5. Conclusions

The multilayer catalyst constructed from carbon fiber, CNT-thin film, polymer-derived silicon carbonitride layer, and finally, a ternary monolayer of precious metals, has reliable and durable performance for generating hydrogen from alkaline, aqueous solutions of sodium borohydride. A clear transition from first order reaction to zero order reaction is demonstrated when the molar concentration of sodium borohydride is increased. The transition to zero order occurs at relative low concentrations of >0.03 M. Since practical systems must be constructed with zero order kinetics (so that the generation rate is independent of the molar concentration), this transition at low molar concentrations can be instrumental in designing systems that avoid precipitation of salts and corrosion.

The first order rate constant, K_1, which is called as the figure-of-merit (FOM), has been determined to have a value of $4600\,L\,min^{-1}\,g_{met}{}^{-1}\,[NaBH_4]^{-1}$, nearly 30 times greater than the values reported in the literature. The zero order rate constant, K_2, which is also known as the hydrogen generation rate (HGR) has been determined to be $75\,L\,min^{-1}\,g_{met}{}^{-1}$. This value is among the top five or six numbers reported in the literature (see Table 2). The catalysts with higher values, however, have far higher loading of precious metals than the present catalyst (more than 10 wt% vs. 0.1 wt%). Additionally the present catalyst is highly reliable and durable, performing reproducibly for many cycles without fading, presumably because the substrate is constructed from covalently bonded Si, C and N. The reliability of the catalysts reported in the literature is not known; these catalysts employ non-stoichiometric oxides such as lithium cobalt oxides that can change their composition by diffusion of lithium at ambient temperature.

The four-layer architecture of the present catalyst has the following design features: a thin film of CNTs, a silicon carbonitride interlayer to disperse the metal atoms into a monolayer, and electronic conductivity, which is needed for the underlying mechanism that has been put forth to explain the catalytic activity [1].

Acknowledgments

The work has been supported by the Dual PhD program between University of Trento, Italy and University of Colorado Boulder (UCB), USA. The research at UCB was supported by a Grant from the Ceramics Program in the Division of Materials Research at the National Science Foundation under Grant No.: 0907108.

References

[1] R. Peña-Alonso, A. Sicurelli, E. Callone, G. Carturan, R. Raj, J. Power Sources 165 (2007) 315–323.
[2] R. Raj, G. Carturan, R. de al Pena-Alonso, Picoscale catalysts for hydrogen catalysis, U.S. Patent application no. 20,090,264,277, pending.
[3] L. Hu, R. Ceccato, R. Raj, Ultrahigh figure-of-merit for hydrogen generation from sodium borohydride using ternary metal catalysts, J. Power Sources, in press (POWER-D-10-01718), Available online 17 July 2010, doi:10.1016/j.jpowsour.2010.07.037.
[4] S.C. Tsang, Y.K. Chen, M.L.H. Green, Nature 372 (1994) 159.
[5] R.M. Lago, S.C. Tsang, M.L.H. Green, J. Chem. Soc. Chem. Commun. (1995) 1355–1356.
[6] W.M. Chiu, Y.A. Chang, J. Appl. Polym. Sci. 107 (2008) 1655–1660.
[7] A. Hirsch, Angew. Chem. Int. Ed. 41 (2002) 1853.
[8] S. Banerjee, Adv. Mater. (January (1)) (2005).
[9] B.J.C. Thomas, A.R. Boccaccini, J. Am. Ceram. Soc. 88 (4) (2005) 980–982.
[10] C. Du, D. Heldbramt, Mater. Lett. 57 (2002) 434–438.
[11] C. Du, N. Pan, J. Power Sources 160 (2006) 1487–1494.
[12] M.S.P. Shaffer, X. Fan, A.H. Windle, Carbon 36 (11) (1998) 1603–1612.
[13] A.R. Boccaccini, J. Cho, Carbon 44 (2006) 3149–3160.
[14] Y. Abe, R. Tomuro, Adv. Mater. 17 (2005) 2192–2194.
[15] B. Gao, G.Z. Yue, Q. Qiu, Y. Cheng, H. Shimoda, L. Fleming, O. Zhou, Adv. Mater. 13 (23) (2001).
[16] S.R. Shah, R. Raj, J. Euro. Ceram. Soc. 25 (2005) 243–249.
[17] T. Teranishi, M. Hosoe, Adv. Mater. 9 (1) (1997).
[18] B.B. Xu, J. Am. Oil Chem. Soc. 84 (2007) 117–122.
[19] M. Zawadzki, Mater. Res. Bull. 43 (2008) 3111–3121.
[20] D. Nagao, Y. Shimazaki, Colloid Surf. A: Physicochem. Eng. Aspects 273 (2006) 97–100.
[21] D.V. Goia, New J. Chem. (1998) 1203–1215.
[22] J.H. Park, P. Shakkthivel, H.J. Kim, M.K. Han, J.H. Jang, Y.R. Kim, H.S. Kim, Y.G. Shu, Int. J. Hydrogen Energy 33 (2008) 1845.
[23] U.B. Demirci, F. Garin, J. Alloys Compd. 5 (2008) 1.
[24] P. Krishanan, K.L. Hsueh, S.D. Yim, Appl. Catal. B 77 (2007) 206.
[25] D. Xu, Y. Hanxi, A. xinping, C. Chuansin, Int. J. Hydrogen Energy 28 (2003) 1095.
[26] C. Wu, H. Zhang, B. Yi, Catal. Today 93 (2004) 477.
[27] P. Krishanan, T.H. Yang, W.Y. Lee, C.C. Kim, J. Power Sources 143 (2005) 17.
[28] R.S. Liu, H.C. Lai, N.C. Bagkar, H.T. Kuo, H.M. Chen, J.F. Lee, H.J. Chung, S.M. Chang, B.J. Weng, J. Phys. Chem. B 112 (2008) 4870.
[29] U.B. Bemirci, O. Akdim, J. Andrieux, J. Hannauer, R. Chamoun, P. Miele, Fuel Cells 10 (3) (2010) 335–350.
[30] Y. Liang, Int. J. Hydrogen Energy 35 (2010) 3023–3028.
[31] C.T. Campbell, Science 298 (2002) 811.
[32] L.M. Falicov, G.A. Somorjai, Proc. Natl. Acad. Sci. U.S.A. 82 (1985) 2207–2211.
[33] J.M. Thomas, W.J. Thomas, Principles and Practice of Heterogeneous Catalysis, VCH, New York, 1997.
[34] J.H. Sinfelt, Acc. Chem. Res. 10 (1977) 15.
[35] W.H.M. Sachtler, Faraday Disc. Chem. Soc. 72 (1981) 7.
[36] G. Ertl, H. Kntizinger, J. Weitkamp (Eds.), Handbook of Heterogeneous Catalysis, Wiley-VCH, New York, 1997.
[37] G.M. Schwab, Disc. Faraday Soc. 8 (1950) 166.
[38] A. Couper, D.D. Eley, Disc. Faraday Soc. 8 (1950) 172.
[39] D.A. Dowden, P. Reynolds, Disc. Faraday Soc. (1950) 184.
[40] J.K.A. Clarke, Chem. Rev. 75 (1975) 291.
[41] V. Ponec, Adv. Catal. 32 (1983) 149.